



## Self-assembly and crystallisation of indented colloids at a planar wall

Journal:	<i>Soft Matter</i>
Manuscript ID:	SM-ART-05-2015-001043
Article Type:	Paper
Date Submitted by the Author:	01-May-2015
Complete List of Authors:	Ashton, Douglas; University of Bath, Department of Physics Ivell, Samantha; University of Oxford, Department of Chemistry Dullens, Roel; University of Oxford, Department of Chemistry Jack, Robert; University of Bath, Department of Physics Wilding, Nigel B.; University of Bath, Department of Physics Aarts, Dirk; University of Oxford, Department of Chemistry

# Self-assembly and crystallisation of indented colloids at a planar wall

Douglas J. Ashton,<sup>a</sup> Samantha J. Ivell,<sup>b</sup> Roel P. A. Dullens,<sup>b</sup> Robert L. Jack,<sup>a</sup> Nigel B. Wilding,<sup>a</sup> Dirk G. A. L. Aarts<sup>\*b</sup>

Received Xth XXXXXXXXXXXX 20XX, Accepted Xth XXXXXXXXXXXX 20XX

First published on the web Xth XXXXXXXXXXXX 200X

DOI: 10.1039/b000000x

We report experimental and simulation studies of the structure of a monolayer of indented (“lock and key”) colloids, on a planar surface. On adding a non-absorbing polymer with prescribed radius and volume fraction, depletion interactions are induced between the colloids, with controlled range and strength. For spherical particles, this leads to crystallisation, but the indented colloids crystallise less easily than spheres, in both simulation and experiment. Nevertheless, simulations show that indented colloids do form plastic (rotator) crystals. We discuss the conditions under which this occurs, and the possibilities of lower-symmetry crystal states. We also comment on the kinetic accessibility of these states.

## 1 Introduction

Self-assembly of colloidal systems is a fast-moving area of current soft-matter research – the synthesis of novel micron-sized particles with controllable anisotropic interactions has allowed the assembly of clusters, “colloidal molecules” and unusual crystals<sup>1–6</sup>. In some cases, anisotropic interactions can be realised by chemical patterning or “patches” on the surface of colloidal particles<sup>5,7–9</sup>. Alternatively, the interplay between particle shape and a depletion interaction can drive self-assembly<sup>3,4,10–14</sup>. One advantage of the depletion interaction is that the strength, range, and specificity of the interaction can be tuned by the properties of the depletant molecules (usually a non-adsorbing polymer), so even a single synthesis of a colloidal system already allows access to a wide range of assembly conditions.

An extra degree of control over self-assembly can be achieved if it takes place under confinement, or at a surface. This effect is particularly strong for anisotropic particles in the presence of depletant, because surfaces can affect the packing of the colloids<sup>15–17</sup>, and depletion forces also acquire an extra orientationally dependent component, associated with binding of the colloids to the surface. These surface effects lead to new possibilities for controllable self-assembly.

Here, we consider “indented” or “lock-and-key” colloids<sup>3,18</sup>. These particles have spherical indentations in their surface, in which similar colloids can fit tightly. This mode of binding is favoured by the depletion effect<sup>11,13,19–21</sup>. We have performed experiments on these particles, and simulated them by a Monte Carlo method. The particles are localised by gravity, against the (bottom) hard wall of their container.

In this setup, simulations and experiments on spherical particles both reveal crystallisation into a hexagonal lattice – this is a very simple example of self-assembly in this colloidal model system. Our main purpose in this paper is to investigate the effect of the shape of the indented colloids on this assembly process. One possibility is that anisotropic particles can lead to crystals with new and different structures<sup>4,22,23</sup>. However, the non-spherical colloidal shape can also disrupt crystal formation, due either to thermodynamic or kinetic factors.

Our results reveal several competing effects. The experiments show clearly that the indentations on the particles act to frustrate crystallisation, and this fact is borne out by the simulations. Similar frustration has been observed before in systems of anisotropic particles<sup>24–26</sup> but in those cases there was significant polydispersity in the particle shapes: here, the experimental polydispersity is small, and the computational system is strictly monodisperse. Moreover, in cases where depletion interactions are not too strong or short-ranged, our simulations do reveal crystallisation of indented particles in a hexagonal lattice, if the model parameters can be “tuned” accurately to the most favorable conditions<sup>27,28</sup>. For stronger interactions, we propose a low-symmetry crystal state that we expect to be stable, but we find that kinetic effects frustrate the assembly of this structure.

Overall, our results allow us to disentangle a variety of effects that impact on the crystallisation of anisotropic colloids. In particular, we find a subtle interplay between thermodynamic and kinetic factors that reinforces the conclusions of previous theoretical studies, that kinetic factors must be borne in mind when designing systems that self-assemble reliably into complex ordered structures<sup>28</sup>.

<sup>a</sup> Department of Physics, University of Bath, Bath BA2 7AY

<sup>b</sup> Department of Chemistry, Physical and Theoretical Chemistry Laboratory, University of Oxford, South Parks Road, Oxford, OX1 3QZ

## 2 Methods

### 2.1 Experiments

The colloidal particles were synthesized following protocols reported in the literature<sup>3,4</sup>. Some modifications were made in order to incorporate a fluorescent dye, rhodamine B isothiocyanate (RITC), for confocal studies<sup>17</sup>. The indented and the spherical particles were made following similar steps: In short, both sets of particles were synthesized from 3-methacryloxypropyl trimethoxysilane (TPM; sourced from Polysciences and used as received). The TPM was hydrolysed under basic conditions, forming a cloudy dispersion of small droplets, which were subsequently grown to the desired size by adding more hydrolysed TPM. Modified RITC was added for fluorescence. At this stage the droplets were either cross-linked from the outside inwards, by adding potassium persulfate (Sigma Aldrich), leading to uniformly indented particles, or, from the inside outwards, by adding azobisisobutyronitrile (BDH Laboratories), which resulted in spherical particles. Both the indented and the spherical particles were made from the same batch of hydrolysed TPM droplets, allowing for a straightforward comparison in the behaviour of both systems. Both sets of particles had a diameter of  $\sigma = 2.56\mu\text{m}$  and a polydispersity of 4%, as measured by static light scattering. The indented particles had a dimple of width  $\sim 1.3\mu\text{m}$  and depth  $\sim 200\text{ nm}$ , as determined by scanning electron microscopy and atomic force microscopy, respectively. Details of the above synthesis method can be found in reference<sup>17</sup>.

The particles were suspended in various aqueous polymer solutions, where the polymers induce a depletion interaction. Specifically, we used solutions of xanthan (molecular weight  $M_w = 3 \times 10^6\text{ g mol}^{-1}$  and calculated radius of gyration  $R_G = 222\text{ nm}$ <sup>29</sup>) and of poly(ethylene oxide) (PEO;  $M_w = 1 \times 10^6\text{ g mol}^{-1}$  and calculated  $R_G = 57\text{ nm}$ <sup>30</sup>), with added salt (0.1M NaCl) to screen the double layer repulsion between the particles. We will focus here on results for PEO; as explained below, the smaller polymer leads to a more specific, directed depletion interaction.

Multiple solutions of colloid-polymer mixtures were prepared in order to study the effect of the concentration of both colloidal particles and polymer in the system. The gravitational length of the colloidal particles was  $0.2\mu\text{m}$ , so they form a colloidal monolayer at the base of the container, with negligible out-of-plane fluctuations. Any fluctuations away from the wall are also suppressed by the depletion interaction between particles and wall. Note that the polymers were not affected by gravity due to their negligible buoyant mass.

Samples were left to sediment completely, which took approximately two hours. The resulting monolayer was then observed using a Zeiss LSM 5 Exciter confocal microscope fitted with a  $63\times$  oil immersion objective. For each sample, movies

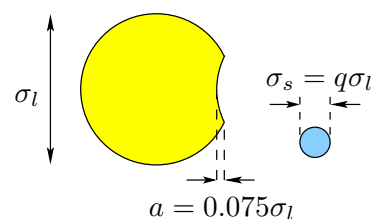


**Fig. 1** Simulation model for the indented colloids. The size ratio between colloidal particles (yellow) and ideal depletant particles (blue) is  $q$ . The indentation depth is fixed at  $a = 0.075\sigma_l$  throughout this work, for consistency with the experimental system.

of 150 frames were recorded, where each frame was  $51.2\mu\text{m} \times 51.2\mu\text{m}$  in size. The 2D coordinates of each particle were found using a tracking routine. In contrast to our recent work on mono-layers in three-dimensional systems of indented colloids<sup>17</sup>, where particles were tightly packed and translational motion was strongly reduced, we were not able to reliably determine particles' orientations in this system.

Due to the sedimentation of the particles, the variables of interest were the colloidal area fraction and the polymer volume fraction. The colloidal area fraction was obtained by counting the number of colloids  $N$  within the area of view  $A$ , and calculating the fraction of the area  $A$  covered by the colloids,  $\phi_c = N\pi\sigma^2/(4A)$ . Here, we will focus on results for a system with a colloidal area fraction of  $\phi_c \approx 0.5$ , and with polymer volume fractions of  $\phi_p \approx 0.5$ .

### 2.2 Simulations

We use Monte Carlo (MC) simulations to calculate the equilibrium properties of indented colloids, in the presence of depletion interactions, confined close to a hard wall. We model these particles by taking spheres of diameter  $\sigma_l$ , and cutting away a volume that corresponds to its intersection with a second sphere of the same diameter. The resulting situation is shown in Fig. 1: the distance between the centres of the spheres is  $d_c = 0.85\sigma_l$ , so the depth of the indentation is  $0.075\sigma_l$ , comparable with the experimental case (approximately  $0.078\sigma$ ). The depletant is modelled as a fluid of small spheres of diameter  $\sigma_s$ , which we parameterise by the size ratio  $q = \sigma_s/\sigma_l$ . These spheres are an 'ideal' depletant<sup>31</sup>: they interact with the colloids as if they were hard particles, but they do not interact with each other. The chemical potential of the depletant is adjusted so that their volume fraction in a system without colloids would be  $\eta_s$ . This modelling approach provides a simple and computationally-efficient model that accurately captures the properties of colloid-polymer mixtures<sup>32–34</sup>.

We place  $N = 100$  colloidal particles in a cuboidal box of

dimensions  $L_x = L_y = 12.5\sigma_l$ ,  $L_z = 2.5\sigma_l$ . Structureless hard walls are placed at  $z = 0$  and  $z = L_z$  and gravity acts in the negative  $z$  direction. These parameters give an area fraction for the colloids of  $\phi_c \approx 0.5$ . The gravitational length associated with the colloidal particles is  $0.1\sigma_l$ , comparable with experiments. Given this gravitational length, the height of the box is sufficient to prevent any effects from the upper wall.

In order to obtain good sampling in this system, we use grand-canonical insertion/deletion moves for the depletant, combined with the geometric cluster algorithm (GCA)<sup>35</sup> as described in<sup>13</sup>. The complete move set includes (i) grand canonical moves for the small particles, (ii) standard displacement and rotation moves of the colloids, (iii) GCA “biased pivot” moves, where the pivot is placed close to the centre of the particle to move it a small distance, (iv) GCA plane moves where a particle can rotate by an arbitrary amount, (v) GCA “biased plane” moves where the particle’s director nearly lies in the reflection plane resulting in a small rotation, and (vi) combinations of pivot and plane GCA moves. At the beginning of the simulations, the colloids are first equilibrated without depletant to ensure they drop to the bottom of the box, after which grand canonical insertion/deletion MC moves for the depletant are turned on

The aim of the GCA is to move clusters of particles together, since otherwise the large number of depletant particles in the system tend to obstruct the movement of the colloids. However, for computational efficiency, it is sometimes convenient to restrict the size of the cluster being moved, since moves of larger clusters require greater computational effort. Therefore, in each Monte Carlo sweep we perform  $N$  moves where the cluster can contain only one indented colloid (but with unlimited depletant particles), as well as one move where the cluster size is unlimited. We perform these moves in 3-dimensions to allow vertical movement of the colloids, but we also perform updates where colloids move only in the  $xy$ -plane, which allows efficient relaxation in two dimensions. Our implementation of the GCA with gravity includes an extra step. As each particle move is proposed, we test for acceptance using a Metropolis criterion, based on the change in gravitational potential energy. If any colloidal particle fails this test the whole move is rejected.

### 2.3 Depletion interactions

The structures that are formed by these indented colloids are controlled by depletion interactions. These interactions arise because if two colloidal particles come close to each other, the volume accessible to the depletant particles is increased. This effect increases the total entropy of the system, and the result is an attractive force between the colloids. There are also attractive depletion forces between the colloids and the hard walls of the system.

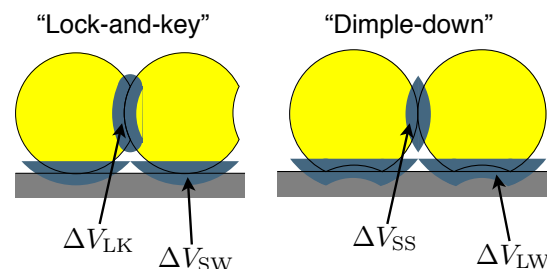


**Fig. 2** Two binding modes for the depletion interaction next to a hard wall (grey). The blue regions indicate the excess free volume  $\Delta V$  that becomes accessible to depletant particles when the colloids bind as shown. The strength of the depletion interaction is proportional to these volumes. In “lock-and-key” binding, one lock sits within the indentation of another, while in “dimple-down” binding, the indentation points towards the wall. Numerical and exact geometrical calculations (see Appendix A) indicate that  $\Delta V_{LK} + \Delta V_{SW} > \Delta V_{SS} + \Delta V_{LW}$ , which means that lock-and-key binding is typically the dominant binding mechanism.

The decrease in free energy (gain in entropy) associated with various configurations of the colloids can be estimated by a geometrical argument. The most relevant cases are illustrated in Fig. 2: they are (a) “lock-and-key” binding, where one colloidal particle sits within the indentation of another colloid; (b) “dimple-down” binding, where the indentation on the colloidal particle points towards a nearby hard wall. The sizes of the shaded areas in Fig. 2 indicate the volume released to the depletant when the colloids bind – the larger the relevant volume, the stronger is the attractive depletion force. These volumes can be calculated geometrically: see Appendix A.

For the purposes of this work, we emphasize two key points. First, the “lock-and-key” binding mechanism is associated with the strongest depletion force, while “dimple-down” binding is rather weaker. The relevant volumes that are released to the depletant are illustrated in Fig. 2: we label these as “lock-and-key” ( $\Delta V_{LK}$ ); “lock-and-wall” ( $\Delta V_{LW}$ ); “sphere-to-sphere” ( $\Delta V_{SS}$ ) and “sphere-to-wall” ( $\Delta V_{SW}$ ). When adding a particle to an existing cluster, “lock-and-key” binding is favoured over “dimple-down” binding if  $\Delta V_{LK} + \Delta V_{SW} > \Delta V_{SS} + \Delta V_{LW}$ . This inequality is satisfied for the particles considered here: see Appendix A.3. Second, the differences in bond strength for the different binding mechanisms are larger when the depletant particles are smaller (small- $q$ ). It may be useful to think of smaller- $q$  corresponding to “more specific” depletion interactions, both in terms of the relative strength of the different bonds, and in terms of the range of the depletion interaction.

### 3 Results

#### 3.1 Structures of spherical and indented colloids

In Fig. 3, we show self-assembled structures in the experimental and computational systems. The colloid area fraction is  $\phi_c \approx 0.5$  in all cases, and there is qualitative agreement between simulation and experiment – while the spherical particles readily crystallise, the indented spheres form large disordered clusters, reminiscent of vapour-liquid coexistence. For comparison, we also show snapshots for experimental systems without any polymer (a,b), where only a liquid-like structure may be observed. In the simulations, the size ratio between colloid and depletant is  $q = 0.125$ , larger than the experimental case; the volume fractions of depletant used in simulation are also lower. This indicates that the depletion interaction in the experiments is weaker than that predicted by the idealised model used in the simulations, which we attribute primarily to non-ideal colloid-depletant interactions<sup>34,36</sup> and (for the indented colloids) an indentation that does not match the perfect spherical shape used in the simulations. However, the qualitative features of the experiments are well captured by the simulations. The dependence of the simulation results on depletant volume fraction is discussed in Section 3.2 below. We also performed experiments using a larger polymer (xanthan). The results are qualitatively similar, in that spheres crystallise more readily than indented colloids.

To quantify the extent of crystallinity and bond-orientational order, we measured the two-dimensional radial distribution function of the colloids  $g(r)$ , as well as a measure of orientational order  $g_6(r)$ . Once the particle positions are known,  $g(r)$  is obtained (as usual) by calculating the distances between all pairs of particles, generating a histogram of these distances  $r$ , and normalising by a factor of  $2\pi rZ$ , where the constant  $Z$  is chosen so that an ideal gas at the same number density would have  $g(r) = 1$ .

To define  $g_6(r)$ , we first introduce a local bond-order parameter for particle  $i$ :

$$\phi_6(i) = \frac{1}{n} \sum_j e^{i6\theta_{ij}} \quad (1)$$

where the sum runs over neighbours  $j$  of particle  $i$ , the number of these neighbours is  $n$  and  $\theta_{ij}$  is the angle between  $\vec{r}_{ij} = \vec{r}_j - \vec{r}_i$  and an arbitrary axis. We define  $\psi_6 = \langle |\phi_6(i)| \rangle$  which provides a simple measure of the local degree of orientational order (the average is independent of  $i$ ). For the spherical particles in Fig. 3(a,b), the snapshots correspond to  $\psi_6 = 0.52$  (without polymer) and  $\psi_6 = 0.67$  (with polymer, PeO at  $\phi_p = 0.5$ ): the crystalline order in Fig. 3(c) is reflected by the local  $\psi_6$  measurement. For indented colloids we have  $\psi_6 = (0.50, 0.49)$ , with and without the polymer (PeO), consistent with the absence of crystalline order in Fig. 3(b,d). For

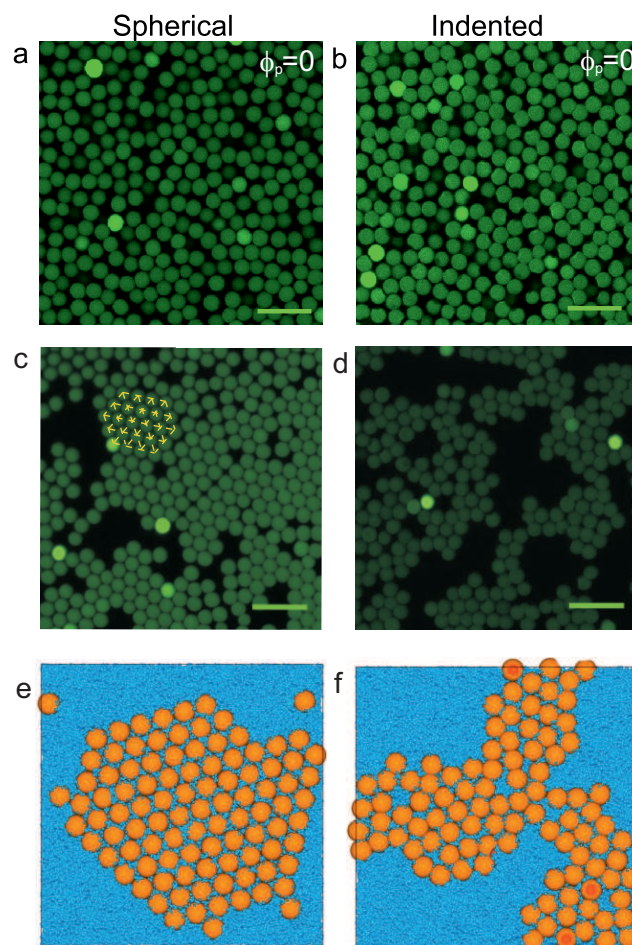


**Fig. 3** Typical configurations of spherical and indented colloids in experiment and simulation. The colloid area fraction is  $\phi_c \approx 0.5$  in all cases. (a-d) Experimental results: the the depletant (not visible) is PEO at volume fraction  $\phi_p = 0.0$  (a,b) and  $\phi_p = 0.5$  (c,d) in a 0.1M salt solution. Samples (a,b) show liquid-like structure. For samples with polymer, the spheres (panel c) form a locally crystalline structure: one domain is highlighted with dashed lines. The indented colloids (panel d) lack this locally crystalline structure. These differences are analysed quantitatively in Fig. 4. Scale bars are  $10\mu\text{m}$ . (e,f) Simulation results: the size ratio is  $q = 0.125$ , which gives qualitative agreement with these experiments. The depletant volume fraction is  $\eta_s = 0.36$ , which was chosen to maximise the crystallinity of the indented sphere system (see Fig. 5 below). As in the experiments, the spheres assemble into a crystalline structure but the indented colloids do not. The simulation snapshots are visualised from below: in (f), there are several particles whose indentations (coloured red) are oriented towards the wall (“dimple-down” configuration).

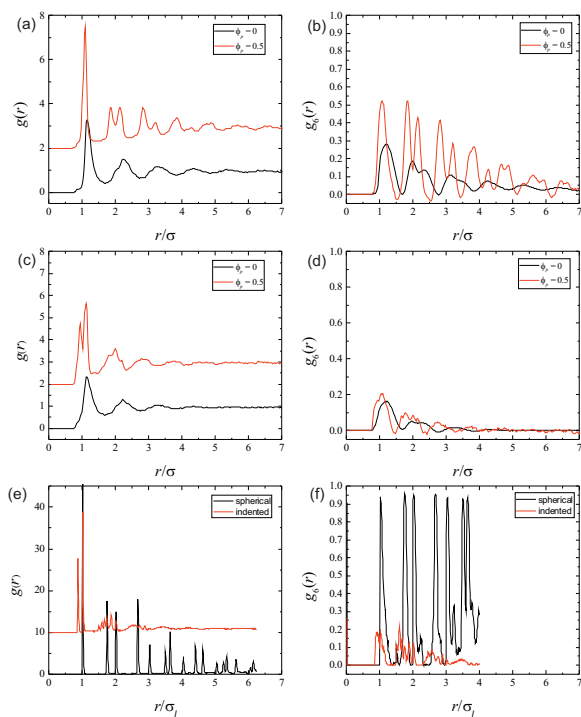


**Fig. 4** Radial distribution functions  $g(r)$  (left column) and orientational correlation function  $g_6(r)$  (right column), under the same conditions as Fig. 3. In some cases the  $g(r)$  data have been shifted vertically, for clarity. Panels (a,b) are experimental results for spherical particles (results are shown with and without depletant). Panels (c,d) are the corresponding results for indented colloids. In the presence of depletant, a peak in  $g(r)$  appears at  $r \approx 0.85\sigma$ , corresponding to lock-and-key binding. The orientational order is weaker for the indented colloids, compared with the spheres. Panels (e,f) show simulation results in the presence of depletant ( $\eta_s = 0.36$ ). The indented colloids show a lock-and-key binding peak in  $g(r)$ , and weaker orientational order than the spheres, consistent with the experiments.

comparison, systems with Xanthan polymer at  $\phi_p = 0.5$  yield  $\psi_6 = 0.75$  (spheres) and  $\psi_6 = 0.50$  (indented colloids), again showing that the spheres crystallise but the indented colloids do not.

To measure order on larger length scales, we use the fact that in systems with bond orientational order, the complex numbers  $\phi_6(i)$  have significant interparticle correlations. In particular,

$$g_6(r) = \frac{\langle \phi_6(i) \phi_6^*(j) \delta(r - |\vec{r}_{ij}|) \rangle}{\langle \delta(r - |\vec{r}_{ij}|) \rangle} \quad (2)$$

measures order at distance  $r$ , with  $g_6(r) = 0$  if the system has no orientational order at length scale  $r$ , while  $g_6(r) = 1$  if the system has perfect bond orientational order. It is also useful to define a ‘‘susceptibility’’, which is related to a spatial integral of  $g_6$ , and gives the approximate size of orientationally-ordered domains in the system:

$$\chi_6 = \frac{1}{N} \left\langle \left| \sum_i \phi_6(i) \right|^2 \right\rangle. \quad (3)$$

Results for positional order [ $g(r)$ ] and orientational order [ $g_6(r)$ ] are shown in Fig. 4. Several features are notable. For  $g(r)$ , the simulation results for spheres (with depletant) show several sharp peaks, consistent with the almost-perfect crystal state shown in Fig. 3. The corresponding data for the indented particles lacks the sharp peaks at  $r > \sigma_l$ , but there is a new peak that appears at  $r \approx 0.85\sigma_l$ . This peak corresponds to the onset of lock-and-key binding for the indented particles: there is a strong depletion force that favours the state where one colloid sits snugly in the indentation of another. The experimental data in the presence of polymer show the same qualitative behaviour: the spheres show a splitting in the second peak of  $g(r)$ , as expected for crystalline states, and there are other peaks in  $g(r)$  for  $r > 2\sigma$ , consistent with crystalline order. It is notable that the peaks in  $g(r)$  are much less sharp for the experiment as compared with the simulation: we attribute this to polydispersity among the colloids, and the inherent uncertainty in capturing particle positions from microscope images. Turning to the experimental data for the indented colloids (with polymer), one observes a suppression of long-ranged positional order (compared with the spheres), and the appearance of a new lock-and-key binding peak at  $r \approx 0.85\sigma$ . In the absence of the polymer, the results of Fig. 4 are consistent with the fluid states shown in Fig. 3(a,b), confirming that depletion interactions are responsible both for the crystallisation of the spheres and for the lock-key binding of the indented colloids.

The orientational correlation function  $g_6(r)$  reinforces this overall picture: the spheres show clear evidence for long-ranged bond-orientational order, as expected for crystalline

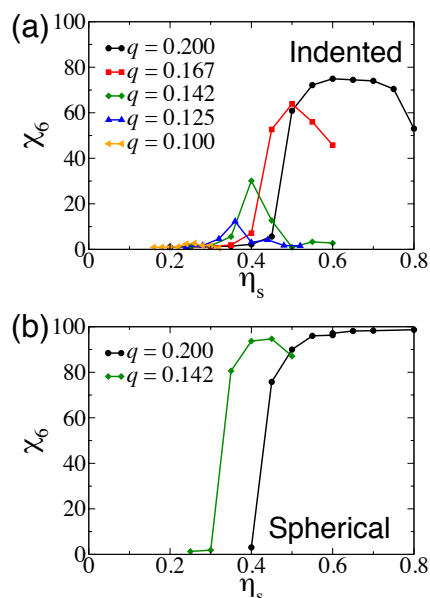


**Fig. 5** Measurements of global bond-orientational order ( $\chi_6$ ) obtained from simulations, as a function of depletant volume fraction  $\eta_s$ , for various sizes ratios  $q$ . Comparing spheres and indented colloids, the spheres crystallise more readily and over a larger range of  $\eta_s$ , although there is evidence for kinetic trapping effects at large  $\eta_s$  and small  $q$ . For the indented colloids, the crystallinity is lower and the range of  $\eta_s$  in which significant crystallisation is observed is much narrower.

states, while the indented particles have shorter-ranged correlations, consistent with the suppression of crystalline order by the lock-and-key bonds. As was clear from  $g(r)$ , the lock-and-key bonds are shorter than the usual sphere-sphere bonds: the presence of two competing length scales for binding acts to suppress the crystalline state. For completeness, we have included results for  $\phi_p = 0$  for the experiments.

Given that both simulation and experimental results indicate that crystallisation is suppressed by indentations in the colloidal particles, we now use simulation studies to investigate this effect in more detail. In particular, we concentrate on the effects of varying depletant size and volume fraction on the indented colloids: by changing the range of the depletion interaction, we are able to tune the system from a state where crystallisation is rapid into a state where crystallisation is frustrated by lock-key binding.

### 3.2 Dependence on depletant size and volume fraction

In Fig. 5, we collate results that show the total amount of orientational order that forms in systems of indented colloids, on varying the size and volume fraction of the depletant. These

results are taken from long MC simulations which were initialised in a disordered state and have “equilibrated” into a steady state – this state is not guaranteed to be the global free energy minimum of the system but it is at least strongly metastable. We discuss this further in Section 3.3 below: the essential point is that if the simulations suffer from strong kinetic effects, it is likely that similar effects will be observed in experiments. So even for systems that are not fully equilibrated, we can expect the metastable states found by simulation to be similar to those found in experiment.

For a size ratio  $q = 0.2$  and  $\eta_s \gtrsim 0.45$ , the system readily crystallises, as is clear from the large values of  $\chi_6$ . The maximum possible value of the susceptibility  $\chi_6$  in a finite system is equal to the total number of particles,  $N = 100$ . One observes  $\chi_6 < N$  either due to local distortions of the crystal lattice, or due to defects and domain boundaries that disrupt the crystalline packing on relatively large length scales. The results for  $q = 0.2$  indicate that the crystal domain size in the system is comparable with the system size. Comparing with the spherical particles, the value of  $\chi_6$  is suppressed: we attribute this primarily to local structural distortion. In this case, we can be confident that the system has equilibrated in its thermodynamically stable state. To reinforce this message, Fig. 6 shows representative configurations: for each size ratio  $q$ , we show a configuration at the point that maximises  $\chi_6$ . The particles are decorated by arrows, which indicate their orientation: the arrow points out through the centre of the indentation in the colloid. At  $q = 0.2$ , the system is indeed crystalline: particles tend to be oriented with their indentations pointing towards adjacent particles, but the range of the interaction is long enough that the crystal is not frustrated. There are also a significant number of dimple-down particles, consistent with this configuration being stabilised by the depletion interaction (but not favoured as strongly as lock-and-key binding). Indeed, comparing with the data for spherical colloids shown in Fig. 5(b) the indentations have rather little effect on the crystallinity. For the largest  $\eta_s$ , the crystallinity starts to fall – we attribute this primarily to kinetic effects: see Sec. 3.3 below.

As  $q$  is decreased, the lock-and-key binding between colloids becomes stronger and shorter ranged, and this starts to disrupt the crystal formation. The onset of crystalline order happens at a lower depletant volume fraction  $\eta_s$ , but the extent of crystalline order is strongly suppressed for  $q < 0.14$ . Fig. 6(b) indicates the origin of this effect: the topology of the particle packing is close to a hexagonal crystal, but the shorter lock-and-key bonds leads to local distortions away from the perfect lattice. (The “crystal planes” deviate from parallel straight lines, reducing orientational order.) For larger  $\eta_s$ , the crystallinity decreases, which we again attribute primarily to kinetic effects.

For the smallest  $q$ , we see almost no evidence of crystallinity. For these small depletant particles, the lock-and-key

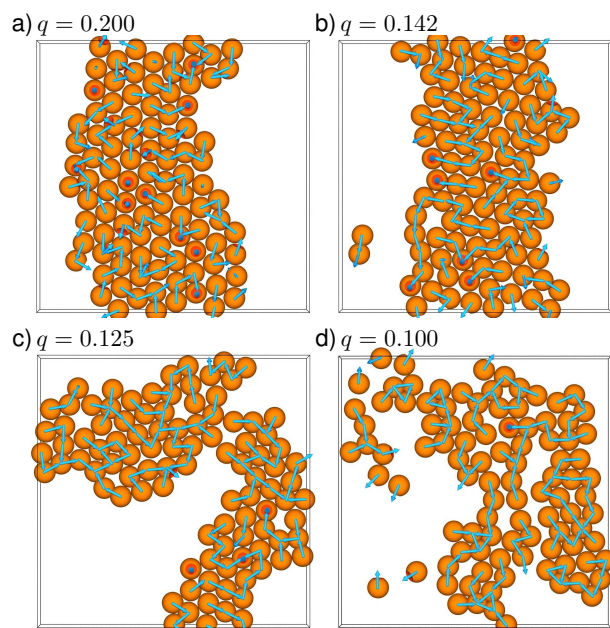


**Fig. 6** Representative configurations from simulations of indented colloids, taken at the values of  $\eta_s$  at which  $\chi_6$  is maximal in Fig. 5. Colloidal orientations are illustrated using arrows pointing outward through the indentations. For  $q = 0.2, 0.142$ , the colloidal orientations relax quickly on the simulation time scale, indicating that this is a plastic (rotator) crystal. For smaller  $q$ , the orientational relaxation is much slower, consistent with the strong lock-and-key binding.

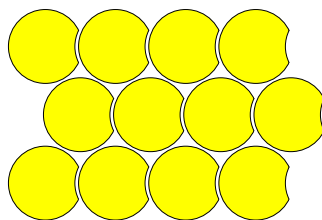


**Fig. 7** Illustration (view from above) of the low-symmetry crystal that we expect to be stable when depletion interactions are very strong. The orientations of the colloids acquire long-ranged order, which breaks the six-fold rotational symmetry of the original crystal – the “lock-and-key” bonds parallel to the orientational order are shorter than the other interparticle bonds.

binding of the colloids is very strong, which leads to strong kinetic trapping<sup>27,37</sup>. Hence, self-assembly of ordered structures tends to be suppressed: this effect is apparent in both simulations and experiments. Nevertheless, we can use theoretical arguments to obtain the expected fate of the system for small  $q$ . We expect the strong lock-and-key binding in this regime to cause the formation of chains of colloids (“colloidal polymers”), which can also branch, leading (when bonds are strong) to large percolating clusters. For small- $q$ , the depletion interaction between the convex surfaces of the colloids is much weaker than the lock-and-key binding, so we expect a range of  $\eta_s$  over which these branching chains dominate the system. However, for larger  $\eta_s$ , the chains can reduce their free energy by clustering (or collapsing in on themselves) – for the largest  $\eta_s$  we expect the stable state to be a low-symmetry crystal such as that shown in Fig. 7. It is interesting to note that neither the simulations nor the experiments solved the packing problem by turning the indentations towards the wall; although this would allow a perfect hexagonal packing, the loss in the depletion interaction compared to the lock-and-key binding is apparently too large for the systems studied here.

### 3.3 Kinetic effects, and stability of low-symmetry crystals

As noted in the previous section, there are significant kinetic trapping effects in these systems, due to the presence of strong directional bonds. For example, in simulations at increasing depletant volume fraction  $\eta_s$ , one observes from Fig. 5 that the crystallinity of the assembled state increases for small  $\eta_s$ , before decreasing again. Such non-monotonicity is familiar from other systems with strong kinetic trapping<sup>27,37,38</sup>. However, in this system, such a non-monotonicity might also arise from purely thermodynamic considerations – the hexagonal crystal may be unstable for very large  $\eta_s$ , due to the presence of two different length scales (shorter lock-and-key bonds and longer bonds between the convex surfaces of colloidal particles).

To distinguish between these kinetic and thermodynamic effects, we performed simulations where the system was initialised in the low-symmetry crystal state shown in Fig. 7, and then relaxed using the GCA as before. This highly-ordered initial state was chosen to contrast with the original “self-assembly” simulations where the system was initialised in a disordered state. Results are shown in Fig. 8. For relatively large  $q$  and small  $\eta_s$ , the simulations gave the same results, independent of the initial condition. As discussed in Section 3.2 above, the MC simulations that we use do not provide direct dynamical information about the experimentally-relevant assembly pathway. However, if the results of the system are independent of initial conditions, this is good evidence that kinetic trapping effects are weak, and the system is fully equi-

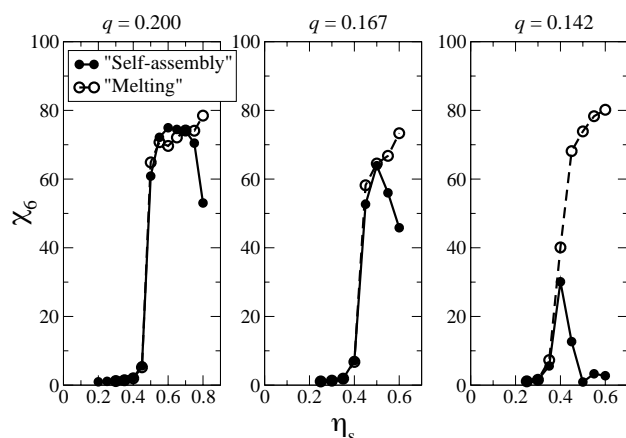


**Fig. 8** Illustration of kinetic effects in MC simulations. We show the extent of bond-orientational order, measured via  $\chi_6$ , obtained from the final states of “self-assembly” simulations (initialised in disordered states, closed symbols) and “melting” simulations (initialised in the low-symmetry crystal shown in Fig. 7, open symbols). For  $q = 0.2$ , the two initial conditions typically lead to similar results, showing that kinetic effects are small and the system readily equilibrates in a plastic (rotator) crystal. For smaller  $q$  and large  $\eta_s$ , the results of the simulation depend strongly on the initial condition, indicating that kinetic effects are strong (see the main text for a full discussion).

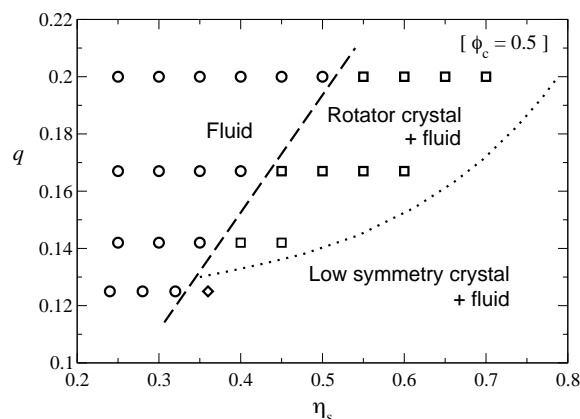


**Fig. 9** Diagram showing observed phase behaviour in simulations of indented colloids (all at colloid area fraction  $\phi_c = 0.5$ ). Our results provide evidence for a simple fluid state (circles) as well as coexistence between the fluid and a hexagonal ‘rotator’ (plastic) crystal (square symbols). These possibilities are familiar from studies of spherical particles (recall Figs. 3(c) and 6(a)). For small  $q$  and large  $\eta_s$ , we expect a low-symmetry crystal such as that shown in Fig. 7 to coexist with the fluid. Self-assembly of this crystal was not observed in our simulations, but systems initialised in this state indicate that it is stable at  $(q, \eta_s) = (0.125, 0.36)$  (diamond symbol). The dashed line is our estimate of the freezing line, and the dotted line indicates the expected location of the transition between rotator and low-symmetry crystals. They meet at a (conjectured) triple point. As discussed in the text, there are considerable uncertainties in the positions of these thermodynamic phase boundaries, due to kinetic/sampling effects in our simulations. However, we expect the general picture presented here to be robust.

librated. We also note that for  $q = 0.2$ , the orientationally-ordered crystalline initial state does relax to a plastic (“rotator”) crystal, providing further evidence that this is the thermodynamically stable state under these conditions.

On the other hand, in the regime of large  $\eta_s$ , simulations initialised as a crystal were observed to evolve to a state whose degree of crystallinity increased with  $\eta_s$ . This contrasts with the non-monotonic behaviour observed in the “self assembly” simulations. In this case, the qualitative dependence of the MC results on the choice of initial condition indicates that kinetic trapping effects are strong: the assembly of crystals from a disordered fluid state is hindered by kinetic effects<sup>28,39,40</sup>. (The possibility of conducting these kinds of thought-experiment reinforces the usefulness of MC simulation in understanding the experimentally-observed behavior of this system.)

In the presence of these kinetic trapping effects, we cannot obtain accurate estimates of the relative stabilities of the ordered phases of the system. However, if we assume that the

simulations started in crystalline states mirror the thermodynamically stable phases, we obtain the qualitative phase behaviour shown in Fig. 9. Hysteresis effects mean that there is considerable uncertainty in the locations of these (presumably) first-order phase transitions, but we expect this general picture to be correct. Accurate studies of phase behaviour in this system would be facilitated by the use of an effective model of colloid-colloid and colloid-wall interactions<sup>31,41</sup>: the very large number of depletant particles required in the simulations used here makes them unsuitable for detailed investigations of phase behaviour.

## 4 Conclusions

Our results show that crystallisation of indented colloids is controlled by a range of factors, including kinetic effects, and a competition between (at least) two different crystal structures. In experiments, the main difference between indented colloids and spheres is that the indented colloids do not crystallise. In simulations, the same trend is observed, but we were able to identify a range of parameters for which crystallisation of indented colloids is observed, when the depletant particles are not too small, and the depletion forces not too strong. We emphasise that this requires the depletant properties to be tuned quite accurately, a situation familiar from other self-assembly processes. The ability of MC simulation to rapidly explore parameter-space through independent parallel computations was useful in this regard; by contrast, crystallisation of indented colloids was not observed in the experiments. Possibilities for ‘tuning’ systems towards a narrow regime of effective assembly has been discussed recently, but this remains a challenging problem<sup>42–44</sup>.

The qualitative agreement between the experimental and simulation results indicates that the model system described here captures the essential features of the experimental system – the suppression of crystallisation in indented colloids can be captured by a simple model of the depletion interaction, in a monodisperse colloidal system.

We have proposed that the low-symmetry crystal shown in Fig. 7 should be thermodynamically stable in the limit where depletion forces are strong and short-ranged. However, while this phase was stable within our simulations, its self-assembly was not observed, presumably due to kinetic effects. The behaviour of the system in this regime remains an interesting area for study.

Finally, we compare the kinetic trapping effects observed here with the physics of colloidal glasses and gels<sup>32,45,46</sup>. While there are superficial connections between glassy behaviour and kinetic trapping in self-assembly, we emphasise that glasses are associated with a metastable liquid phase, which is homogeneous in space, and has very slow structural relaxation. Such a situation might be possible for anisotropic

colloids in three dimensions<sup>26</sup> but we do not see evidence here for a metastable liquid state. Rather, the situation for indented colloids is more similar to gelation, in which attractive particles aggregate into disordered clusters. This analogy is most useful for very strong and short-ranged depletion interactions (see for example Fig. 6(d)): similar considerations are relevant for three-dimensional crystallization<sup>39</sup>. For more moderate values of  $q$  (for example Fig. 6(b,c)), the behaviour of this two-dimensional system more closely resembles a polycrystal with extremely small domains. That is, most particles are six-fold coordinated as in the crystal, but long-ranged orientational and positional order is disrupted by a very large number of packing defects.

## Acknowledgments

We are grateful to the EPSRC for support for DJA and NBW through grant EP/I036192/1; a PhD studentship (for SI); and support for RLJ through grant EP/I003797/1.

## A Calculations of excess free volume $\Delta V$

This appendix gives expressions for the volumes of the shaded regions in Fig. 2, which determine the strength of depletion interactions for different modes of binding. We make extensive use of a formula for the volume of a ‘spherical cap’:

$$V_{\text{cap}}(D, h) = \frac{\pi}{6} h^2 (3D - 2h) \quad (4)$$

where  $D$  is the diameter of the underlying sphere and  $h$  the height, as shown in Fig. 10.

### A.1 Sphere-sphere and sphere-wall

The cases of spheres interacting with each other and with walls are well-known. The calculation follows that of Asakura and Oosawa<sup>31</sup>, considering an ideal depletant of diameter  $\sigma_s = q\sigma_l$ . As may be seen from Fig. 2, the sphere-sphere depletion volume  $\Delta V_{\text{SS}}$  consists of two spherical caps. These caps are formed from the intersection of two spheres of diameter  $\sigma_l + \sigma_s$ , with their centres separated by  $\sigma_l$ . (The spheres represent the volume that the spherical colloid (diameter  $\sigma_l$ ) excludes from the centre of the depletant particle (diameter  $\sigma_s$ )). The heights of the spherical caps are therefore  $\sigma_s/2$ . Hence

$$\Delta V_{\text{SS}} = 2V_{\text{cap}}(\sigma_l + \sigma_s, \sigma_s/2) \quad (5)$$

We are interested in cases where  $q = \sigma_s/\sigma_l$  is small (compared to unity) in which case

$$\Delta V_{\text{SS}} \approx \frac{\pi q^2}{4} \sigma_l^3 \quad (6)$$

which holds to leading order in  $q$ .

Similarly the sphere-wall excluded volume is a single spherical cap of diameter  $\sigma_l + \sigma_s$  and height  $\sigma_s$ , yielding

$$\Delta V_{\text{SW}} = V_{\text{cap}}(\sigma_l + \sigma_s, \sigma_s) \approx \frac{\pi q^2}{2} \sigma_l^3 \quad (7)$$

where as before the approximate equality is accurate to leading order in  $q$ . For small  $q$ , the sphere-wall interaction is around twice as strong as the sphere-sphere interaction.

In terms of the effective potential between colloids, the well depth is given by the product of the number density of depletant and the relevant  $\Delta V$  factor. Writing this in terms of the volume fraction of depletant for the sphere-sphere case, we have

$$\varepsilon_{\text{SS}} \approx \frac{3\eta_s}{2q} \quad (8)$$

This equation emphasises that the interactions get stronger on reducing  $q$  (at constant  $\eta_s$ ).

## A.2 Indented colloid excluded volume

Calculation of the volumes  $\Delta V_{\text{LK}}$  and  $\Delta V_{\text{LW}}$  in Fig. 2 are a little more involved. The main difficulty is accurate calculation of the volume excluded to a depletant particle by a single indented colloid. This calculation can be performed exactly but we give an approximate treatment here, as illustrated in Fig. 10. As is clear from that figure, the error involved in this approximation is small, and it greatly simplifies the analysis.

Within this approximation, the volume excluded by a single lock is obtained by subtracting two spherical caps from the volume of a sphere of diameter  $\sigma_l + \sigma_s$ . The two spherical caps are associated with spheres of diameter  $\sigma_l \pm \sigma_s$ , and the sum of their heights is  $2a$ , where the parameter  $a$  was defined in Fig. 1. Ensuring that the diameters of the circular areas of both caps are equal (recall Fig. 10) yields that the cap heights are  $h_{\pm} = a[1 \pm (\sigma_s/(\sigma_l - 2a))]$ . Hence the volume excluded to a depletant particle by a lock is  $(\pi(\sigma_l + \sigma_s)^3/6) - \Delta V_{\text{L}}$  with

$$\Delta V_{\text{L}} = V_{\text{cap}}(\sigma_l + \sigma_s, h_-) + V_{\text{cap}}(\sigma_l - \sigma_s, h_+) \quad (9)$$

After some algebra, this may be simplified, yielding

$$\Delta V_{\text{L}} = 2V_{\text{cap}}(\sigma, a) - \frac{\pi\sigma_s^2 a^2}{\sigma - 2a}. \quad (10)$$

With this result in hand, the calculation of the volumes  $\Delta V_{\text{LK}}$  and  $\Delta V_{\text{LW}}$  in Fig. 2 is straightforward. For two indented particles (“lock-key” binding), the excluded volume is given by two spherical caps, with the volume  $\Delta V_{\text{L}}$  removed from one of them. The spherical caps have diameters  $\sigma_l + \sigma_s$  and their heights are  $(\sigma_s/2) + a$ . Hence

$$\Delta V_{\text{LK}} = 2V_{\text{cap}}(\sigma_l + \sigma_s, (\sigma_s/2) + a) - \Delta V_{\text{L}} \quad (11)$$

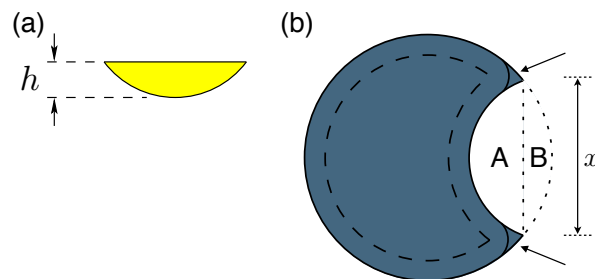


**Fig. 10** Geometrical objects used in the calculation of excess free volumes. (a) Cross section of a spherical cap; the height parameter  $h$  used in the main text is indicated. The radius of curvature of the curved part is  $D/2$ . (b) Illustration of the volume excluded to the centre of an ideal depletant particle by an indented colloid. The particle outline is shown as a dashed line. The shaded blue region is our estimate of the volume excluded to the depletant. The actual volume excluded may be obtained by “rolling” a small sphere around the edge of the colloid: this is indicated by the (inner) solid line. The small difference between the blue shaded area and the actual exclusion volume occurs in the region indicated by the arrows. The labels A and B indicate spherical caps corresponding to the difference between the blue region and a large sphere of diameter  $\sigma_l + \sigma_s$ . The radius of curvature of cap B is  $(\sigma_l + \sigma_s)/2$  while that of cap A is  $(\sigma_l - \sigma_s)/2$  (the relevant surfaces are parts of spheres that are concentric with the surfaces of the indented colloid). Using the fact that the radius of curvature of the concave surface of the lock is  $\sigma_l/2$ , one may show that the sum of the heights of caps A and B is  $2a$ . Both spherical caps have the same width  $x$ , as indicated.

From (10), one readily sees that  $\Delta V_{LK}|_{\sigma_s=0} = 0$ , as it should be. If both  $q = \sigma_s/\sigma_l$  and  $a_0 = a/\sigma_l$  are small compared to unity, the dominant term is

$$\Delta V_{LK} \approx \pi q(a_0 + q/4)\sigma_l^3 \quad (12)$$

For  $a_0 = 0$  we recover the sphere-sphere result (6); the lock-key result is significantly larger as soon as  $a_0$  becomes comparable with  $q/4$ .

For an indented particle against a wall, the simplest case occurs when  $a < \sigma_s$ , so that a depletant particle cannot fit into the dimple of a colloid that is flat against the wall. In this case the relevant volume is a single spherical cap with the volume  $\Delta V_L$  subtracted,

$$\Delta V_{LW} = V_{\text{cap}}(\sigma_l + \sigma_s, \sigma_s + a) - \Delta V_L. \quad (13)$$

On the other hand for  $a > \sigma_s$  it is easily verified that

$$\Delta V_{LW} = V_{\text{cap}}(\sigma_l + \sigma_s, \sigma_s + a) - \Delta V_L + V_{\text{cap}}(\sigma_l - \sigma_s, a - \sigma_s) \quad (14)$$

For  $q, a_0 \ll 1$ , one finds

$$\Delta V_{LW} \approx (\pi/2)(q^2 + 2a_0q - a_0^2)\sigma_l^3, \quad a_0 < q \quad (15)$$

$$\approx \pi q^2 \sigma_l^3, \quad a_0 > q. \quad (16)$$

### A.3 Competition between binding modes

As discussed in the main text, when depletion interactions are strong then lock-key binding will dominate over dimple-down if  $\Delta V_{LK} + \Delta V_{SW} > \Delta V_{SS} + \Delta V_{LW}$ . Assuming for convenience that  $\sigma_s > a$  (i.e.,  $q > a_0$ ), this condition reduces to

$$2V_{\text{cap}}(\sigma_l + \sigma_s, (\sigma_s/2) + a) + V_{\text{cap}}(\sigma_l + \sigma_s, \sigma_s) > 2V_{\text{cap}}(\sigma_l + \sigma_s, \sigma_s/2) + V_{\text{cap}}(\sigma_l + \sigma_s, \sigma_s + a) \quad (17)$$

A similar condition holds for  $q < a_0$ , with one extra  $V_{\text{cap}}$  term, as prescribed by (14). After some algebra one may show that this condition is satisfied for all  $0 < q, a < 1$ , so one generally expects lock-key binding to dominate the system when depletion attractions are strong.

## References

- S. C. Glotzer and M. J. Solomon, *Nature Materials*, 2007, **6**, 557–562.
- A. van Blaaderen, *Science*, 2003, **301**, 470–471.
- S. Sacanna, W. T. M. Irvine, P. M. Chaikin and D. J. Pine, *Nature*, 2010, **464**, 575–578.
- L. Rossi, S. Sacanna, W. T. M. Irvine, P. M. Chaikin, D. J. Pine and A. P. Philipse, *Soft Matter*, 2011, **7**, 4139–4142.
- Q. Chen, S. C. Bae and S. Granick, *Nature*, 2011, **469**, 381–384.
- S. Sacanna, L. Rossi and D. J. Pine, *J. Am. Chem. Soc.*, 2012, **134**, 6112–6115.
- D. J. Kraft, J. Groenewold and W. K. Kegels, *Soft Matter*, 2009, **5**, 3823–3826.
- A. B. Pawar and I. Kretzschmar, *Macromolecular Rapid Commun.*, 2010, **31**, 150–168.
- A. H. Groschel, A. Walther, T. I. Lobling, F. H. Schacher, H. Schmalz and A. H. E. Muller, *Nature*, 2013, **503**, 247–251.
- K. Zhao and T. G. Mason, *Phys. Rev. Lett.*, 2007, **99**, 268301.
- G. Odriozola, F. Jimenez-Angeles and M. Lozada-Cassou, *J. Chem. Phys.*, 2008, **129**, 111101.
- D. J. Kraft, R. Ni, F. Smalenburg, M. Hermes, K. Yoon, D. A. Weitz, A. van Blaaderen, J. Groenewold, M. Dijkstra and W. K. Kegels, *Proc. Natl. Acad. Sci. USA*, 2012, **109**, 10787–10792.
- D. J. Ashton, R. L. Jack and N. B. Wilding, *Soft Matter*, 2013, **9**, 9661–9666.
- D. Ortiz, K. L. Kohlstedt, T. D. Nguyen and S. C. Glotzer, *Soft Matter*, 2014, **10**, 3541–3552.
- P. D. Kaplan, J. L. Rouke, A. G. Yodh and D. J. Pine, *Phys. Rev. Lett.*, 1994, **72**, 582–585.
- E. K. Riley and C. M. Liddell, *Langmuir*, 2010, **26**, 11648–11656.
- S. J. Ivel, R. P. A. Dullens, S. Sacanna and D. G. A. L. Aarts, *Soft Matter*, 2013, **9**, 9361.
- S. Sacanna, M. Korpics, K. Rodriguez, L. Colón-Meléndez, S.-H. Kim, D. J. Pine and G.-R. Yi, *Nat Commun*, 2013, **4**, 1688.
- M. Kinoshita and T. Oguni, *Chem. Phys. Lett.*, 2002, **351**, 79–84.
- P.-M. König, R. Roth and S. Dietrich, *EPL*, 2008, **84**, 68006.
- G. Odriozola and M. Lozada-Cassou, *Phys. Rev. Lett.*, 2013, **110**, 105701.
- P. F. Damasceno, M. Engel and S. C. Glotzer, *Science*, 2012, **337**, 453–457.
- N. Khalid Ahmed, G. van Anders, E. R. Chen, and S. C. Glotzer, arXiv:1501.03130.
- R. P. A. Dullens, M. C. D. Mourad, D. G. A. L. Aarts, J. P. Hoogenboom and W. K. Kegels, *Phys. Rev. Lett.*, 2006, **96**, 028304.
- R. P. A. Dullens and A. V. Petukhov, *EPL*, 2007, **77**, 58003.
- R. Rice, R. Roth and C. P. Royall, *Soft Matter*, 2012, **8**, 1163–1167.
- S. Whitelam, E. H. Feng, M. F. Hagan and P. L. Geissler, *Soft Matter*, 2009, **5**, 1251–1262.
- S. Whitelam and R. L. Jack, *Ann. Rev. Phys. Chem.*, **66**, 143 (2015).
- G. H. Koenderink, D. G. A. L. Aarts, V. W. A. de Villeneuve, A. P. Philipse, R. Tuinier and H. N. W. Lekkerkerker, *Biomacr.*, 2003, **4**, 129.
- B. Z. Shang, Z. Wang and R. G. Larson, *J. Phys. Chem. B*, 2008, **112**, 2888.
- S. Asakura and F. Oosawa, *J. Chem. Phys.*, 1954, **22**, 1255–1256.
- W. C. K. Poon, *Journal of Physics: Condensed Matter*, 2002, **14**, R859.
- S. M. Ilett, A. Orrock, W. C. K. Poon and P. N. Pusey, *Phys. Rev. E*, 1995, **51**, 1344–1352.
- H. N. W. Lekkerkerker and R. Tuinier, *Colloids and the Depletion Interaction*, Springer, Dordrecht, 2011.
- J. W. Liu and E. Luijten, *Phys. Rev. Lett.*, 2004, **92**, 035504.
- P. Germain, J. G. Malherbe and S. Amokrane, *Phys. Rev. E*, 2004, **70**, 041409.
- J. Grant, R. L. Jack and S. Whitelam, *J. Chem. Phys.*, 2011, **135**, 214505.
- M. F. Hagan and D. Chandler, *Biophys. J.*, 2006, **91**, 42–54.
- A. Fortini, E. Sanz and M. Dijkstra, *Phys. Rev. E*, 2008, **78**, 041402.
- D. Klotsa and R. L. Jack, *Soft Matter*, 2011, **7**, 6294–6303.
- D. J. Ashton, R. L. Jack and N. B. Wilding, arXiv:1501.07472.
- R. L. Jack, M. Hagan and D. Chandler, *Phys. Rev. E*, 2007, **76**, 021119.
- E. Jankowski and S. C. Glotzer, *Soft Matter*, 2012, **8**, 2852–2859.
- D. Klotsa and R. L. Jack, *J. Chem. Phys.*, 2013, **138**, 094502.
- E. Zaccarelli, *Journal of Physics: Condensed Matter*, 2007, **19**, 323101.
- E. Weeks and D. Weitz, *Physical Review Letters*, 2002, **89**, 095704.